Contrib Mineral Petrol (2001) 141: 66–82
DOI 10.1007/s004100000218

Jörg Hermann · Daniela Rubatto · Andrei Korsakov
Vladislav S. Shatsky

Multiple zircon growth during fast exhumation of diamondiferous, deeply subducted continental crust (Kokchetav Massif, Kazakhstan)

Received: 15 August 2000 / Accepted: 16 October 2000 / Published online: 21 February 2001

Abstract Diamondiferous rocks from the Kokchetav Massif, Kazakhstan, represent deeply subducted continental crust. In order to constrain the age of ultra high pressure (UHP) metamorphism and subsequent retrogression during exhumation, zircons from diamondiferous gneisses and metacarbonates have been investigated by a combined petrological and isotopic study. Four different zircon domains were distinguished on the basis of transmitted light microscopy, cathodoluminescence, trace element contents and mineral inclusions. Mineral inclusions and trace element characteristics of the zircon domains permit us to relate zircon growth to metamorphic conditions. Domain 1 consists of rounded cores and lacks evidence of UHP metamorphism. Domain 2 contains diamond, coesite, omphacite and titanian phengite inclusions providing evidence that it formed at UHP metamorphic conditions ($P > 43$ kbar; $T \sim 950$ °C). Domain 3 is characterised by low-pressure mineral inclusions such as garnet, biotite and plagioclase, which are common minerals in the granulite-facies overprint of the gneisses ($P \sim 10$ kbar; $T \sim 800$ °C). This multi-stage zircon growth during cooling and exhumation of the diamondiferous rocks can be best explained by zircon growth from Zr-saturated partial melts present in the gneisses. Domain 4 forms idiomorphic overgrowths and the rare earth element pattern indicates that it formed without coexisting garnet, most probably at amphibolite-facies conditions ($P \sim 5$ kbar; $T \sim 600$ °C). The metamorphic zircon domains were dated by SHRIMP ion microprobe and yielded ages of 527 ± 5, 528 ± 8 and 526 ± 5 Ma for domains 2, 3 and 4 respectively. These indistinguishable ages provide evidence for a fast exhumation beyond the resolution of SHRIMP dating. The mean age of all zircons formed between UHP metamorphic conditions and granulite-facies metamorphism is 528 ± 3 Ma, indicating that decompression took place in less than 6 Ma. Hence, the deeply subducted continental crust was exhumed from mantle depth to the base of the crust at rates higher than 1.8 cm/year. We propose a two-stage exhumation model to explain the obtained P–T–t path. Fast exhumation on top of the subducted slab from depth > 140 to ~ 35 km was driven by buoyancy and facilitated by the presence of partial melts. A period of near isobaric cooling was followed by a second decompression event probably related to extension in a late stage of continental collision.

Introduction

The finding of coesite (Chopin 1984; Compagnoni et al. 1995) and metamorphic micro diamonds (Sobolev and Shatsky 1990; Shatsky et al. 1995) in rocks derived from continental crust demonstrates that the least dense part of the lithosphere can be buried to 100–150 km depth or more. Whereas subduction of continental crust can account for bringing these rocks to great depth, it is more difficult to understand how these rocks were exhumed to the Earth's surface. One fundamental factor to understand the dynamics of exhumation of UHP rocks is time because the exhumation rate can be a crucial parameter to distinguish between different exhumation processes (Ring et al. 1999). However, the calculation of exhumation rates requires accurate determination of age and pressure in metamorphic rocks. The classical approach to this problem has been by dating a series of minerals, which have

Supplementary Table 1 is part of electronic supplementary material only. It has been deposited in electronic form and can be obtained from http://dx.doi.org/10.1007/s004100000218.

J. Hermann (✉) · D. Rubatto
Research School of Earth Sciences, Australian National University, Canberra, ACT 0200, Australia
E-mail: joerg.hermann@anu.edu.au

A. Korsakov · V. S. Shatsky
United Institute of Geology, Geophysics and Mineralogy, Novosibirsk 630090, Russia

Editorial responsibility: J. Hoefs

different, presumably known, closing temperatures (e.g. Hunziker et al. 1992). Through an inferred pressure–temperature (PT) relationship, time could then be linked to pressure. Although this approach might be successful in slowly exhumed and slowly cooled granulite facies rocks, it is infeasible for HP rocks because they underwent near-isothermal decompression, preventing a reliable correlation of temperature with pressure. An alternative approach is to date formation ages of minerals with high closure temperatures such as zircon (Lee et al. 1997). The main problem to solve then is the link between the zircon age and the metamorphic evolution of the rock unit.

One key area to study exhumation of deeply subducted continental crust is the Kokchetav Massif in Kazakhstan where diamond-bearing metamorphic rocks occur (Fig. 1). Previous dating of the Kokchetav rocks has provided some constraints on the age of metamorphism but lacks the resolution and details needed in order to shed light on the exhumation of the diamondiferous rocks. Claoue-Long et al. (1991) produced an age of 530 ± 7 Ma by ion microprobe (SHRIMP) U–Pb dating of zircons with diamond inclusions. A diamond aggregate was found to be situated between a zircon core and rim. As core and rim were part of the 530-Ma population, Claoue-Long et al. (1991) concluded that this age dates the time of diamond formation. However, their study was not assisted by cathodoluminescence imaging or petrography of inclusions other than diamond and, therefore, no constraints on the exhumation of the diamond-bearing rocks were presented. Sm–Nd dating of these rocks (Shatsky et al. 1999) has been largely compromised by garnet zoning and widespread retrogression. The best constrained isochron is defined by minerals separated from an eclogite and yields an age of 535 ± 3 Ma (Shatsky et al. 1999). However, it is unclear if this age dates formation or cooling because the rock has experienced temperatures of up to 950 °C. Additional information about the retrograde evolution comes from ^{39}Ar–^{40}Ar dating of muscovite and biotite, which indicates cooling below the isotopic closure of these minerals at 517 ± 5 and 515 ± 5 Ma (Troesch and Jagoutz 1993; Shatsky et al. 1999).

In this paper we present a detailed combined isotopic and petrological study of metamorphic zircon from the diamondiferous rocks in the Kokchetav Massif. In order to link zircon growth to metamorphic conditions, we first constrained the retrograde P–T path for the diamondiferous rocks based on own and literature data. The zircons have been characterised on the basis of transmitted light microscopy, cathodoluminescence, trace element geochemistry and mineral inclusions. Four different zircon domains have been identified and dated in-situ by SHRIMP ion microprobe. The petrology of mineral inclusions and the trace element patterns of zircon permit us to relate zircon growth to metamorphic conditions. We propose a two-stage exhumation model in order to explain the obtained P–T–t path for the retrograde evolution of the diamondiferous rocks. Additionally, the petrological information of zircon growth, combined with the study of radiogenic isotopes and trace element contents of zircon, permits insight into the behaviour of this key mineral during high temperature–high pressure (HT–HP) metamorphism.

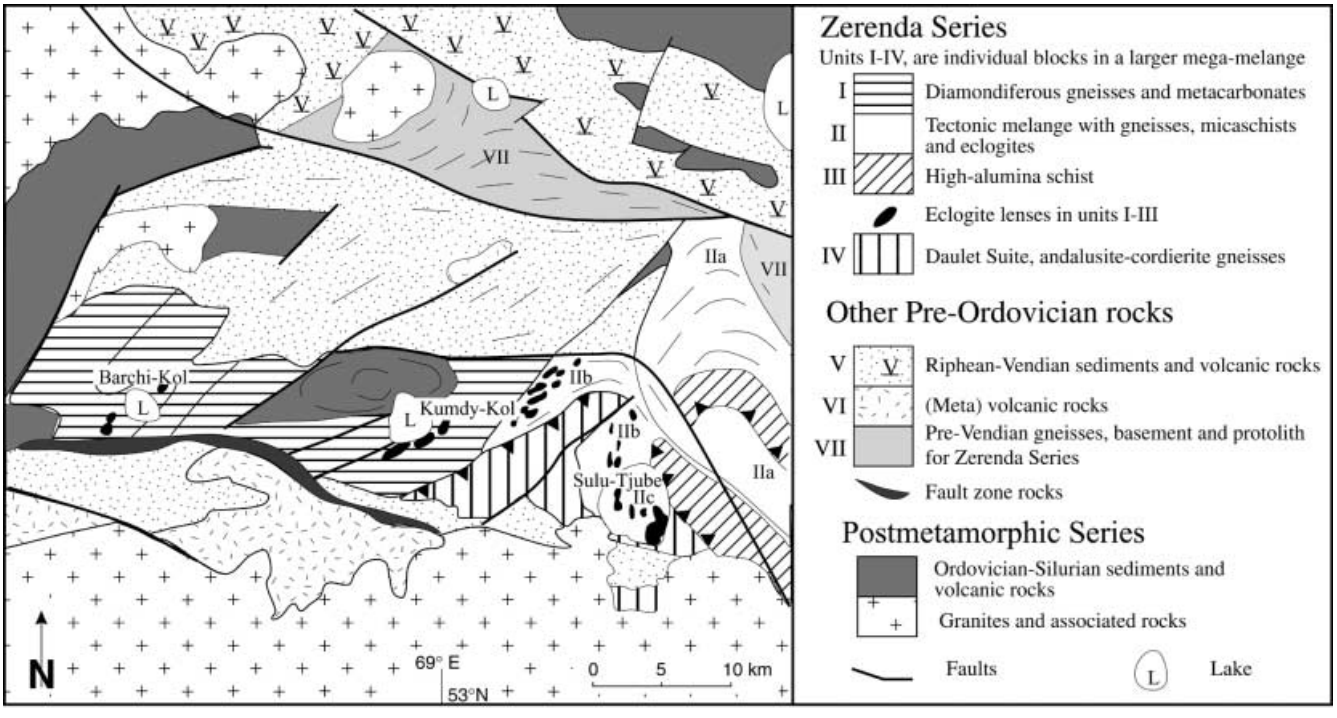

Fig. 1 Simplified geological map of the Kokchetav Massif after Dobretsov et al. (1995)

Geological setting and sample description

The Kokchetav Massif forms part of the Caledonian Central-Asiatic fold belt and is situated between the Siberian platform and the East European platform in Kazakhstan (Dobretsov et al. 1995). This massif has become known worldwide because of metamorphic micro diamonds being found, providing evidence for UHP (>40 kbar) metamorphism (Sobolev and Shatsky 1990; Shatsky et al. 1995). The diamondiferous rocks are present in unit I of the Zerenda Series, which consists mainly of garnet–biotite–kyanite gneisses and schists with intercalated dolomitic marbles, calc-silicates and eclogites (Fig. 1; Dobretsov et al. 1995). The rock association in the Zerenda Series has been related to the formation of a passive continental margin predating subduction (Dobrzhinetskaya et al. 1994). Diamonds have been found in all rock types of unit I except eclogites and migmatites (Shatsky et al. 1995). The unit I diamondiferous rocks make up part of a mega-melange (Fig. 1; Dobretsov et al. 1995) consisting of rocks types exhibiting contrasting metamorphic conditions. Unit II (Fig. 1) also contains HP to UHP relics (Shatsky et al. 1998a); however, peak temperature (720–760 °C) and pressure (P ~ 34–36 kbar) seem to be significantly lower than in unit I (Parkinson 2000). Unit IV contains rocks with cordierite and andalusite, which are characteristic of low-pressure (LP)–HT metamorphism (3 kbar; 650 °C; Dobretsov et al. 1995).

We dated zircons from various gneisses and from a dolomitic metacarbonate sampled at the classical Barchi-Kol locality in unit I (Fig. 1, Sobolev and Shatsky 1990; Shatsky et al. 1995, 1999). A detailed list of the mineral assemblage as well as of inclusions found in zircon are given in Table 1 and selected mineral compositions are shown in Tables 2 and 3. Kyanite gneisses are fine grained and consist mainly of garnet and kyanite porphyroblasts in a biotite, K-feldspar and quartz matrix. Biotite gneisses display the assemblage garnet, biotite, feldspar and quartz with minor amounts of clinopyroxene and plagioclase. Zircon is a common accessory mineral and variable amounts of carbonates are present in all gneisses. Diamonds are generally found as inclusions in garnet and zircon. The dolomitic metacarbonate consist of large garnets and K-bearing clinopyroxenes embedded in a dolomite matrix. Garnet and clinopyroxene both contain diamond inclusions.

Analytical techniques

Mineral compositions were determined with a JEOL 6400 scanning electron microscope (Electron Microscopy Unit, Australian National University) and a Cameca Camebax Electron Microprobe (Research School of Earth Sciences, Australian National University) using an energy dispersive detector. Analytical conditions were 15 kV, 1 nA and 15 kV, 5–6 nA respectively. Further analyses were made in the X-ray laboratory, United Institute of Geology, Geophysics and Mineralogy, SB RAS, with a Camebax Electron Microprobe using WDS and working conditions of 20 kV, 20 nA and 20 kV, 10 nA for rock-forming minerals and inclusions respectively.

Zircons were prepared as mineral separates, mounted in epoxy and polished down to expose the grain centres. The selection of zircons for isotope and trace element analyses was done on the basis of the cathodoluminescence (CL) images. CL investigation was performed on a HITACHI S2250-N scanning electron microscope at the Electron Microscope Unit, Australian National University.

Zircon trace element analysis was performed on the Laser-Ablation-ICP-MS at the RSES in Canberra (Eggins et al. 1998). Ablation was done with a pulsed 193 nm ArF Excimer laser with 100 mJ energy at a repetition rate of 5 Hz and pits size of 30 μm. A mixed Ar–He stream was used to transport the aerosol into the Fisons PQ2 + ICP-MS where 22 masses were analysed. Detection limits were in the order of 0.05 ppm for REE.

Zircon was analysed for U, Th and Pb using the sensitive, high-resolution ion microprobe SHRIMP II at the Research School of Earth Sciences. Instrumental conditions and data acquisition were generally as described by Compston et al. (1992). The data were collected in sets of seven scans throughout the masses and a reference zircon was analysed each fourth analysis. The measured $^{206}Pb/^{238}U$ ratio was corrected using reference zircon from a gabbro of the Duluth Complex in Minnesota (AS3). The data were corrected for common Pb on the basis of the measured $^{207}Pb/^{206}Pb$ and assuming a Broken Hill common lead composition, which approximates the laboratory common lead at RSES. Ages on single data points are quoted at a 1σ level, whereas mean ages are given at a 95% confidence level.

An OMARS 89 (Dilor, France) Raman spectrometer equipped with a Nicon microscopy was used for Raman spectra accumulation (Institute Mineralogy and Petrography SB RAS, Novosibirsk).

Table 1 Main mineral assemblage in the samples dated and mineral inclusions found in the separated zircons. Minerals in *bold* represent UHP inclusions, *italics* refer to clear low-pressure inclusions. *Grt* Garnet; *Ky* kyanite; *Bt* biotite; *Phe* phengite; *Ti-phe* titanium-rich phengite; *Ms* muscovite; *Qtz* quartz; *Kfs* K-feldspar; *Pl* plagioclase; *Chl* chlorite; *Cal* calcite; *Dol* dolomite; *Cpx* clinopyroxene; *Dia* diamond; *Cs* coesite; *Rt* rutile; *G* graphite

Sample	Mineral assemblage	Inclusions in zircons
Gneisses		
B93-168	Grt–Ky–Bt–Phe–Kfs–Qtz	**Dia**, Ky, Rt, Kfs, Qtz, G, *Phe*, *Bt*
B93-9	Grt–Bt–Kfs–Qtz–Chl	**Dia**, G, Grt
B93-161	Grt–Bt–Kfs–Pl–Qtz–Cal–Chl	**Dia**, **Ti-Phe**, **Cs**, **Cpx**, Grt, G
B94-24	Grt–Ky–Bt–Kfs–Qtz–Chl	**Dia**, **Ti-Phe**, G, Grt, Ky, Rt, Qtz
B94-15	Grt–Ky–Bt–Phe–Kfs–Qtz–Ms	**Cs, Ti-Phe**, Grt, Qtz, *Bt*
B94-299	Grt–Ky–Bt–Pl–Qtz–Chl	**Grt**, **Cpx**
B94-175	Grt–Ky–Bt–Phe–Kfs–Pl–Qtz–Chl	**Cs, Ti-Phe**, Grt, Rt, Qtz, *Phe*, *Pl*, *Ab*, *Chl*
Metacarbonate		
C1	Grt, Cpx, Dol, Bt ± K-phase	**Dia**, **Grt**, Dol

Table 2 Representative analyses from diamondiferous rocks showing different stages of retrograde equilibration (see Fig. 2). *Car1* Dolomitic metacarbonate; *G2* biotite–amphibole–pyroxene–garnet gneiss; *GQ1* garnet–biotite–phengite–gneiss. Minerals co-existing together have the same superscript letter. $Grt_{C,I,R}$ Analyses made in core, intermediate zone and rim of garnet, respectively. Garnet compositions are normalised on 12 cations and 24 charges, pyroxene on 12 charges (Fe^{3+} free), plagioclase on 5 cations and 16 charges, amphibole on Σ(*cat*)–K–Na–Ca = 13 and 46 charges, and mica on 22 charges. The H_2O content of hydrous phases is calculated from the mineral formula

Stage	UHP (A)		Granulite facies (B)				Amphibolite facies (C)						(D)	
Sample	Car1		G2				GQ1						GQ1	
Mineral	Grt[a]	Cpx[a]	Grt[b]	Cpx[b]	Grt[c]	Am[c]	Grt_c	Grt_I[d]	Bt[d]	Grt_R[e]	Phe[e]	Pl[e]	Grt_r[f]	Pl[f]
SiO_2 wt%	40.7	54.6	38.7	52.3	37.8	41.7	37.4	37.5	37.5	38.0	48.0	62.8	37.7	57.1
TiO_2	0.24	< 0.08	0.20	0.10	0.14	0.41	0.16	< 0.07	1.95	0.13	1.03	< 0.08	< 0.08	< 0.08
Al_2O_3	22.3	0.96	21.3	3.14	20.8	14.8	21.0	20.7	17.2	21.3	30.5	23.4	20.8	27.1
Fe_2O_3	1.33		3.41		3.10	1.10	3.18	2.62		2.86			0.19	
FeO	6.68	1.49	19.2	6.20	20.4	13.1	24.2	22.9	15.6	17.9	1.90	0.51	23.3	0.29
MnO	0.67	< 0.09	1.38	< 0.09	1.65	0.35	4.64	4.20	0.27	4.35	< 0.09	< 0.09	10.7	0.18
MgO	10.0	16.4	7.16	12.9	4.99	10.1	4.58	4.22	12.21	3.24	2.10	< 0.08	3.13	0.11
CaO	18.5	25.3	10.2	24.3	11.2	12.64	6.06	7.90	0.10	13.7	< 0.06	4.94	3.85	9.27
Na_2O	< 0.16	< 0.16	< 0.16	0.65	< 0.16	0.84	< 0.16	< 0.16	< 0.15	< 0.16	< 0.16	8.53	< 0.16	6.10
K_2O	< 0.04	0.62	< 0.04	< 0.04	< 0.04	1.74	< 0.04	< 0.04	9.82	< 0.04	11.2	0.17	< 0.04	0.15
H_2O						2.00			4.00		4.45			
Σ Cations	100.4	99.5	101.6	99.6	99.9	98.8	101.2	100.1	99.0	101.4	99.2	100.4	99.8	100.5
Si	2.986	1.996	2.938	1.945	2.946	6.260	2.928	2.960	2.810	2.939	3.234	2.779	3.015	2.558
Ti	0.013		0.011	0.002	0.008	0.046	0.009		0.110	0.008	0.052			
Al	1.928	0.041	1.906	0.138	1.910	2.619	1.938	1.925	1.548	1.941	2.420	1.220	1.965	1.431
Fe3	0.074		0.195		0.182	0.124	0.187	0.155		0.167			0.012	
Fe2	0.410	0.046	1.221	0.193	1.330	1.646	1.587	1.514	0.977	1.153	0.107	0.019	1.561	0.011
Mn	0.042		0.089		0.109	0.045	0.308	0.281	0.017	0.285			0.722	0.007
Mg	1.094	0.895	0.810	0.716	0.580	2.260	0.535	0.496	1.366	0.373	0.211		0.374	0.007
Ca	1.454	0.991	0.830	0.966	0.935	2.033	0.508	0.668	0.008	1.135		0.234	0.330	0.445
Na				0.047		0.245						0.732		0.530
K		0.029				0.333			0.938		0.966	0.010		0.009
OH						2.000			2.000		2.000			
Σ		3.998		4.007		15.61			7.774		6.990			

Table 3 Comparison between compositions of mineral inclusions in zircon and mineral compositions in the main assemblage. Abbreviations and formula calculation as in Table 2

	Inclusions in zircon								Minerals in main paragenesis									
Sample	B94-299		B94-15		B94-24		B93-161		B94-299		B94-15		B94-24			B93-161		
Stage	A	A	B	B–C	B–C	A	A	A	B	C	B–C	B–C	B–C	B–C	B–C	B–C	B–C	B–C
Mineral	Grt	Cpx	Grt	Grt	Grt	Phe	Phe	Cpx	Grt_C	Grt_R	Gr_C	Grt_R	Grt_C	Gr_R	Bt	Grt_C	Grt_R	Bt
SiO_2	40.2	52.8	39.0	39.1	38.9	49.0	50.7	54.8	39.7	39.6	39.1	39.1	38.7	38.4	37.0	40.1	39.6	38.2
TiO_2	0.08	0.45	< 0.08	< 0.08	< 0.08	2.73	1.49	0.19	0.03	0.02			0.09	0.02	2.59	0.03	0.00	2.05
Al_2O_3	22.3	12.0	22.1	21.8	22.0	25.1	26.1	12.8	21.7	21.7	21.3	21.3	21.3	21.3	17.8	22.4	22.0	16.8
Fe_2O_3			1.63	0.07														
FeO	15.0	2.74	21.1	21.3	25.0	2.28	1.97	2.75	19.74	17.4	22.2	22.3	26.9	26.5	14.8	17.5	20.0	13.2
MnO	0.76	0.21	0.42	0.85	0.45	< 0.09	< 0.09	0.20	1.11	1.08	0.47	0.45	1.63	1.68	0.12	0.72	1.41	0.32
MgO	11.5	10.4	8.37	6.85	8.70	4.12	4.51	9.13	9.86	8.26	7.51	7.48	8.62	7.86	12.9	10.63	9.21	15.5
CaO	8.84	17.0	7.93	9.64	4.10	< 0.06	< 0.06	15.2	7.95	11.8	9.23	9.24	2.97	4.27	0.00	9.16	8.00	0.02
Na_2O	< 0.16	3.40	< 0.16	< 0.16	< 0.16	< 0.16	< 0.16	5.00	0.02	0.04			0.06	0.05	0.17	0.04	0.05	0.19
K_2O	< 0.04	< 0.04	< 0.04	< 0.04	< 0.04	11.3	9.85	< 0.04	0.00	0.01			0.00	0.00	9.26	0.00	0.02	9.33
H_2O						4.39	4.48								4.02			4.08
Σ Cations	98.7	99.0	100.6	99.7	99.2	98.9	99.1	100.1	99.9	99.9	99.9	99.9	100.2	100.1	98.8	100.4	100.3	99.6
Si	3.02	1.90	2.96	3.01	3.01	3.34	3.39	1.94	3.01	3.01	3.01	3.01	2.99	2.98	2.76	2.99	3.00	2.81
Ti	0.01	0.01				0.14	0.07	0.01			0.00	0.00	0.01		0.15	0.00	0.00	0.11
Al	1.98	0.51	1.98	1.98	2.01	2.02	2.06	0.53	1.93	1.94	1.93	1.93	1.94	1.95	1.58	1.97	1.97	1.45
Fe_3			0.09	0.00														
Fe_2	0.94	0.08	1.34	1.37	1.62	0.13	0.11	0.08	1.25	1.11	1.43	1.43	1.74	1.72	0.92	1.09	1.27	0.81
Mn	0.05	0.01	0.03	0.06	0.03			0.01	0.07	0.07	0.03	0.03	0.11	0.11	0.01	0.05	0.09	0.02
Mg	1.29	0.56	0.95	0.79	1.00	0.42	0.45	0.48	1.12	0.93	0.86	0.86	0.99	0.91	1.43	1.18	1.04	1.70
Ca	0.71	0.65	0.65	0.80	0.34			0.58	0.65	0.96	0.76	0.76	0.25	0.36	0.00	0.73	0.65	0.00
Na		0.24						0.34							0.02	0.01	0.01	0.03
K						0.98	0.84								0.88	0.00	0.00	0.88
OH						2.00	2.00								2.00			2.00
Σ		3.96				7.03	6.92	3.97							7.75			7.81

Excitation was provided by the 514.53 nm line of an Ar-ion laser (ILA-120-1, Carl Zeiss, German) at 20–50 mW, focused to a spot size 1.5 μm. Spectra were measured with spectrometer entrance slits at 100 μm, with a 2-s counting time at 0.5 wave-number steps. The resolution of spectral bands was 0.5 cm^{-1}. Analysed samples were single polished zircon grains mounted in epoxy.

Pressure–temperature data

Peak UHP metamorphism

The most reliable data about peak metamorphic diamond-facies conditions stems from diamond itself. The metamorphic diamonds of the Kokchetav Massif contain nitrogen impurities in the form of singly substituted C-centres (type Ib) as well as nitrogen in pairs (type IaA; Taylor et al. 1996; De Corte 2000). As the transition from Ib to IaA diamond is a function of temperature and time, Taylor et al. (1996) concluded that the diamonds from the Kokchetav Massif experienced peak temperatures of $\sim$ 950 °C (Fig. 2) and were not longer than about 17 Ma above temperatures of 750 °C. Diamonds in different rock types display distinct populations of cuboid to cuboctahedral shapes (Shatsky et al. 1998b; De Corte 2000). The dependence of diamond morphology on rock types strongly argues for an in-situ metamorphic formation of the diamonds (De Corte 2000). Hence, a minimum pressure of 43 kbar for the formation of the Kokchetav diamonds is constrained by the graphite to diamond transition (Fig. 2).

The dolomitic metacarbonates preserve widespread mineralogical evidence for UHP metamorphism. K-bearing (0.5–1.5 wt%) clinopyroxene (Shatsky et al. 1995; Zhang et al. 1997) co-exists with grossular-rich garnet, and garnet–clinopyroxene thermometry yields 950–1,000 °C (Fig. 2), in agreement with temperatures deduced from diamonds. In contrast, the main paragenesis in the gneisses (Table 1) indicates retrograde equilibration at upper amphibolite to granulite-facies conditions (see below). However, UHP minerals such as diamond, coesite, omphacite and titanium-rich phengite (Ti-phengite) occur as inclusions in garnet, kyanite (Shatsky et al. 1995) and zircon (Table 1), providing evidence for a common metamorphic evolution of all investigated samples.

Decompression and partial melting

Garnet in the dolomitic metacarbonate displays a large unzoned core and narrow rims with decreasing Ca and increasing Mg contents. The Ca content in garnet is probably buffered by the co-existing carbonate by the equilibrium 3 $dolomite^{car}$ + $grossular^{grt}$ = 6 $calcite^{car}$ + $pyrope^{grt}$, which has dolomite + grossular on the HP side. It is therefore suggested that the observed garnet zoning reflects decompression (Fig. 2). Similar zoning has been observed in some garnets of the zoisite gneisses (Korsakov 2000). This is in contrast to the normal

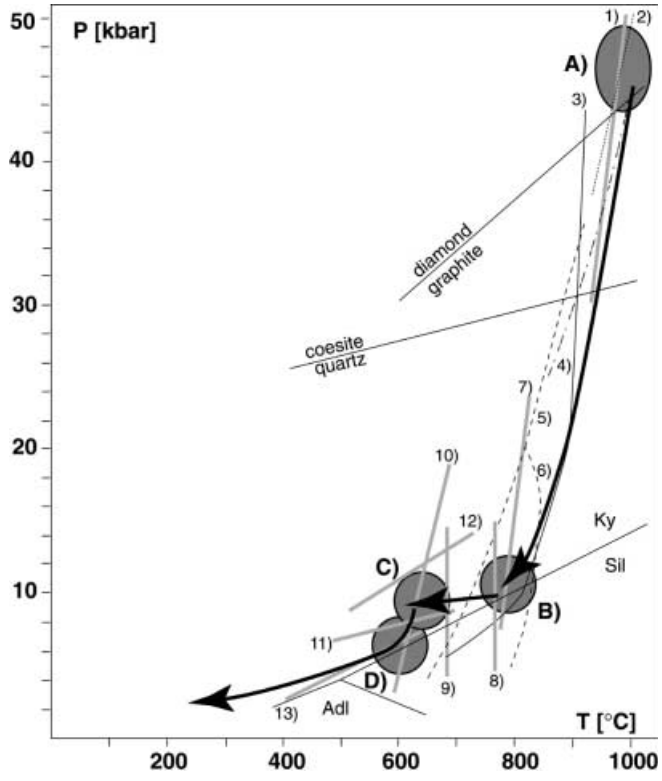

Fig. 2 P–T path of the Kokchetav diamondiferous rocks. Major stages of recrystallisation: *A* UHP-peak metamorphic conditions; *B* granulite-facies overprint; *C* amphibolite facies overprint; *D* amphibolite facies decompression. Graphite–diamond transition after Kennedy and Kennedy (1976); quartz–coesite transition after Mirwald and Massone (1980); Al_2SiO_5-polymorph stability after Holdaway (1971). *1* Garnet–clinopyroxene thermometry (Ellis and Green 1979) for UHP dolomitic metacarbonate Car1. Melt producing reactions in pelitic to granitic compositions. *2* Fluid-absent melting in metagreywackes and metapelites (Schmidt and Vielzeuf 2000). *3* Melt-in boundary from a metapelite (Patiño Douce and McCarthy 1998). *4* phengite melting in KCMASH (Hermann and Green 2000). *5* Phengite melting and *6* biotite melting in the presence of quartz and kyanite in metagreywackes and metapelites with $X_{Mg}\sim0.5$ (Vielzeuf and Holloway 1988). *7* Garnet–clinopyroxene (Ellis and Green 1979) and *8* garnet–amphibole (Graham and Powell 1984) thermometry for upper amphibolite- to granulite-facies gneiss (G1). *9–13* Amphibolite-facies conditions obtained from gneiss GQ1: *9* garnet–biotite thermometry (Indares and Martignole 1985) for biotite inclusion in garnet with intermediate Ca content; *10* garnet–phengite thermometry (Green and Hellman 1982) for phengite co-existing with Ca-rich garnet rim; *11* Si content of phengite co-existing with biotite, K-feldspar, and quartz (Massonne and Schreyer 1987); *12* calculated equilibrium grossular + muscovite + quartz = K-feldspar + anorthite + water with Berman (1988) database, mixing model for plagioclase (Fuhrman and Lindsley 1988), garnet (Berman 1990), ideal mixing muscovite and $a(H_20)=1$. The metamorphic conditions of amphibolite facies stage C are defined by *9–12*. *13* Maximum pressure for stage D is indicated by the equilibrium grossular + Al_2SiO_5 + quartz = anorthite with $a(Al_2SiO_5) \leq 1$ using the Berman (1988) database and mixing model for plagioclase (Fuhrman and Lindsley 1988) and garnet (Berman 1990). An error of ± 50 °C and ± 1 kbar has to be considered for all thermobarometers. Representative analyses of the minerals are given in Table 2. See text for discussion

garnet zoning in the gneisses where the Ca increases from core to rim (Tables 2 and 3; Shatsky et al. 1995). Experiments in pelitic bulk rock composition from 20–45 kbar indicate that, in plagioclase-free rocks, i.e. at eclogite facies conditions, the Ca contents of garnet co-existing with clinopyroxene and kyanite decreases with pressure at a constant temperature (Hermann and Green 1999). Consequently, the increase in Ca contents in the garnets from the gneisses is not consistent with decompression from UHP conditions and must reflect a later event in the metamorphic evolution (see below).

The main reason for the poor preservation of UHP conditions in the gneisses is probably the presence of partial melts during decompression from diamond- to granulite-facies conditions. This whole P–T segment is situated at higher temperatures than experimentally determined for fluid-absent melting in similar bulk compositions (Fig. 2). The dominant fluid-absent melting reaction is probably phengite + clinopyroxene + coesite → garnet + kyanite + melt, which produces a hydrous granitic melt (Hermann and Green 2000). This would explain why UHP phases are only preserved in kyanite, garnet and zircon, which are the main restitic minerals. Unfortunately, the textures of the gneisses cannot be used to prove this hypothesis because of the subsequent, nearly pervasive granulite-facies overprint. However, as the extraction of granitic melt changes the mode and bulk rock composition of the residue, these characteristics help to decide whether or not partial melting occurred. The diamond-bearing gneisses are often biotite-poor, garnet, clinopyroxene, kyanite and quartz-rich gneisses that probably represent strongly melt-depleted rock types. Diamond-bearing gneisses are characterised by depletion in K, Na and Si and concomitant passive enrichment in Ca and Mg (Shatsky et al. 1995), which is consistent with melt extraction. Further evidence for melt extraction stems from the depletion in light rare earth elements (LREE) of the diamond-bearing gneisses (Shatsky et al. 1999). Therefore, the mode and bulk rock composition of the diamond-bearing gneisses support the existence of significant partial melting in the diamond-bearing gneisses.

Granulite-facies metamorphism

The main mineral assemblage in the gneisses consists of garnet, clinopyroxene, amphibole, biotite, K-feldspar and plagioclase (Table 1), which is characteristic of upper amphibolite to granulite-facies conditions. Thermometry of a biotite–amphibole–pyroxene–garnet gneiss (Fig. 2) yields consistent temperatures of ~ 800 °C. This is in agreement with a temperature of 790 °C deduced from garnet–biotite thermometry of retrograde phases in a dolomitic metacarbonate (Zhang et al. 1997). In the kyanite gneisses, the transformation of kyanite to sillimanite has not been observed, indicating that kyanite is probably stable over the whole retrograde evolution and constrains minimum pressure to about 10 kbar for the granulite-facies overprint.

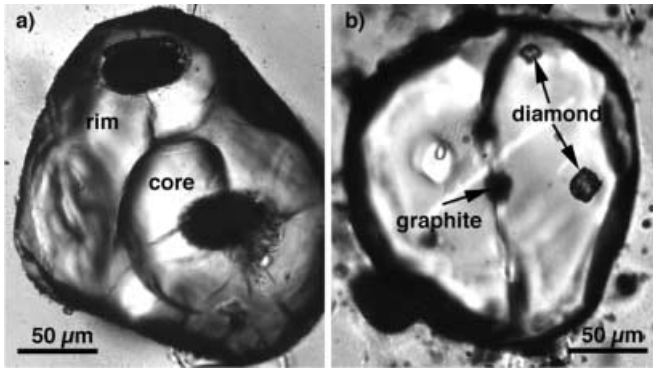

Fig. 3 Transmitted light image of zircons. **a** A rounded zircon core is overgrown by a rim. The black ovals are pits of the LA-ICP-MS analyses. In this case, the core was not perfectly hit by the laser (zircon KYG 24-1, sample B94-299). **b** Diamond inclusions in zircon. One diamond situated in a crack of the zircon is pseudomorphically replaced by graphite (zircon KYG 2-3, sample B93-168)

Isobaric cooling and amphibolite-facies metamorphism

Garnet zoning in the gneisses is generally characterised by an increase in Ca contents from core to rim (Tables 2 and 3; Shatsky et al. 1995; Korsakov 2000). The grossular content of garnet co-existing with plagioclase, alumosilicate and quartz is buffered by the equilibrium anorthite = kyanite + quartz + grossular, which has a positive slope and anorthite on the LP side (Ghent 1976). This equilibrium is very useful to distinguish between isobaric cooling and isothermal decompression in granulite-facies terrains because the resulting garnet zoning is different. A Ca increase in garnets coexisting with plagioclase is a characteristic feature of near-isobaric cooling from granulite facies to upper amphibolite facies in lower crustal rocks (Hermann et al. 1997). We suggest that the observed Ca increase in garnets co-existing with plagioclase in the Kokchetav gneisses can best be explained by nearly isobaric cooling. Garnets showing such chemical zoning, even if they contain diamond inclusions, must have completely re-equilibrated at granulite-facies conditions and do not preserve information about UHP metamorphism and subsequent decompression.

The P–T conditions at the end of near isobaric cooling can be estimated from a garnet–biotite–phengite–gneiss (Table 2). The presence of phengite, which is not stable in the granulite-facies paragenesis (Fig. 2), indicates equilibration at amphibolite facies conditions. Garnet–biotite thermometry applied to biotite inclusions in garnet domains with intermediate Ca-contents yields temperatures of ~ 700 °C (Fig. 2), consistent with cooling from granulite- to amphibolite-facies conditions. Phengite co-exists with the Ca-rich garnet rim, and garnet–phengite thermometry yields temperatures of ~ 650 °C (Fig. 2). At this temperature, a pressure of ~ 10 kbar is constrained by the composition of unzoned plagioclase (An_{25}) in contact with garnet rims (Grs_{36}), which co-exist with phengite, K-feldspar and quartz (Fig. 2). A Si content of 3.25 in phengite (Table 2), co-existing with K-feldspar, biotite and quartz indicates pressures of ~ 8 kbar (Fig. 2). These P–T estimates together with the observed garnet zoning suggest that isobaric cooling occurred at $\sim 9 \pm 2$ kbar.

Amphibolite facies decompression

There is clear evidence for further decompression post-dating the pressure-dominated amphibolite facies conditions. The Ca-rich garnets occasionally have a 10–20-μm small rim that is poor in Ca and Mg, and rich in Mn (Table 2). This garnet co-exists with plagioclase, displaying a significantly higher anorthite content (An_{45}). Biotite and K-feldspar rims around phengite provide further evidence for decompression. The paragenesis with K-feldspar, plagioclase, biotite and garnet indicates amphibolite facies conditions, i.e. temperatures of ~ 550–600 °C. At this temperature, a maximum pressure of ~ 5 kbar is constrained by garnet and plagioclase compositions (Table 2). The growth of chlorite and the widespread decomposition of garnet probably during significant fluid influx documents further retrograde metamorphism post-dating the amphibolite-facies equilibration.

Zircon characterisation

The zircons are generally isometric and display a soccer-ball shape, as is often observed in HT metamorphic terrains (e.g. Vavra et al. 1996). Zircon has been characterised by transmitted light microscopy (TL; Fig. 3), CL (Fig. 4), and trace element composition (Fig. 5) as well as by its inclusions (Fig. 6, Tables 1 and 3). On the basis of this information, four main zircon domains have been distinguished.

Domain 1: cores

Rounded cores visible in TL (Fig. 3a) are either free of inclusions or contain LP minerals such as chlorite and plagioclase and are occasionally surrounded by rims containing diamonds (Fig. 4a). The cores are generally weakly zoned in CL and their internal zoning pattern is crosscut by later rims (Fig. 4a, b). REE patterns of domain 1 are clearly different from those of domains 2–3 and display much higher LREE contents and slightly higher heavy-(H)REE contents (Fig. 5a).

The presence of LP inclusions and the absence of diamond inclusions suggest the formation of domain 1 prior to diamond-facies metamorphism. The observation that zircon cores retain a different REE pattern than metamorphic zircon domains (see below) demonstrates that some of the trace elements were not equilibrated at peak metamorphic conditions. Claoue-Long et al. (1991) found widespread evidence of inherited

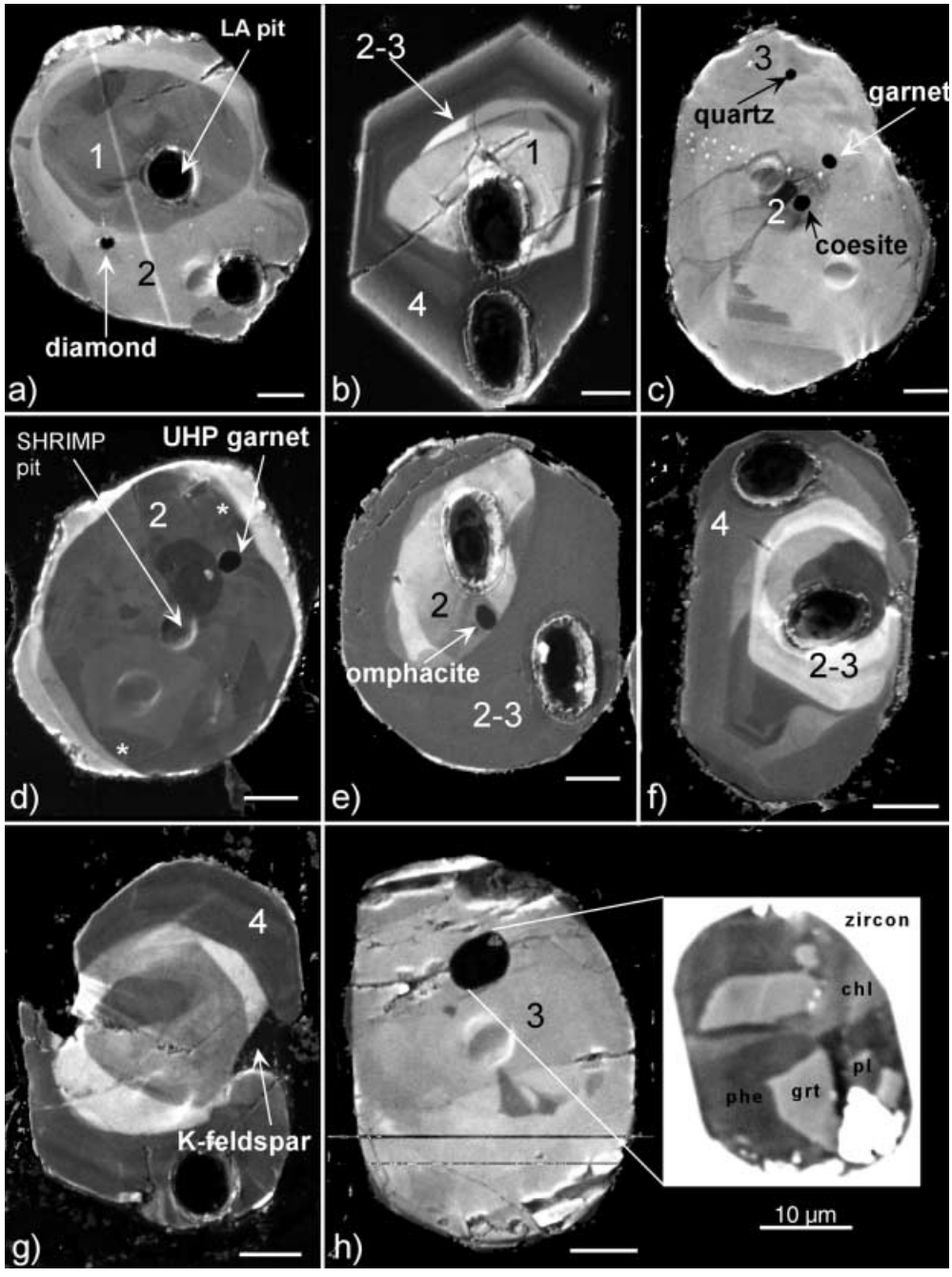

Fig. 4 Cathodoluminescence images of zircon. The *scale bar* is 25 µm if not otherwise indicated. **a** Zircon KYG14-1 (sample B94-24) with a domain 1 core surrounded by domain 2, which contains a diamond inclusion. **b** Zircon KYG18-3 (sample B94-15) with a domain 1 core visible in CL and transmitted light. The core has a high Th/U ratio of 0.15. The euhedral, dark rim has an REE composition typical of domain 4. **c** Zircon KYG18-1 (sample B94-15) with inclusions of coesite and garnet in domain 2 and an inclusion of quartz in domain 3. Note that domains 2 and 3 are not distinguishable on the basis of the CL image only. **d** Zircon KC11-2 (dolomitic metacarbonate) with inclusions of UHP garnet and diamond. * Diamond visible in transmitted light. **e** Zircon KYG24.3 (sample B94-299) with an inclusion of omphacite in the core. REE composition of core and rim is similar. **f** Zircon BTG4-2 (sample B93–9) with a euhedral domain 4 rim surrounding a core with REE composition typical of domains 2–3. **g** Zircon KYG1-1 (sample B93-168) with a domain 4 rim with an inclusion of K-feldspar. **h** Zircon KYG24-2 (sample B94-299) with a multiple inclusion containing a granulite to amphibolite-facies assemblage

zircons (apparent ages 558–1,981 Ma), which pre-dated metamorphism from a biotite schist coming from the Kumdy-Kol locality (Fig. 1). It could therefore be possible that domain 1 represents relics of detrital zircon from a meta-sedimentary protolith. Alternatively, the cores were formed during prograde metamorphism before UHP conditions were reached.

Domain 2: UHP zircon

Coesite inclusions in zircon (Fig. 4c) have been identified by Raman spectroscopy (Fig. 7). These inclusions provide unambiguous evidence for zircon growth at UHP conditions. UHP formation of zircon is further supported by the presence of diamond inclusions (Fig. 3b) because diamond is not stable during retrogression and is transformed to graphite (Shatsky et al. 1995). Even in zircon, which is generally the best container to preserve diamond, graphitisation of diamond has been observed along microcracks (Fig. 3b).

In the dolomitic metacarbonates, garnet and dolomite included in domain 2 zircon (Fig. 4d) have the same composition as in the UHP paragenesis, which indicates zircon growth at peak metamorphic conditions. Ti-rich phengite inclusions in zircons from gneisses have higher

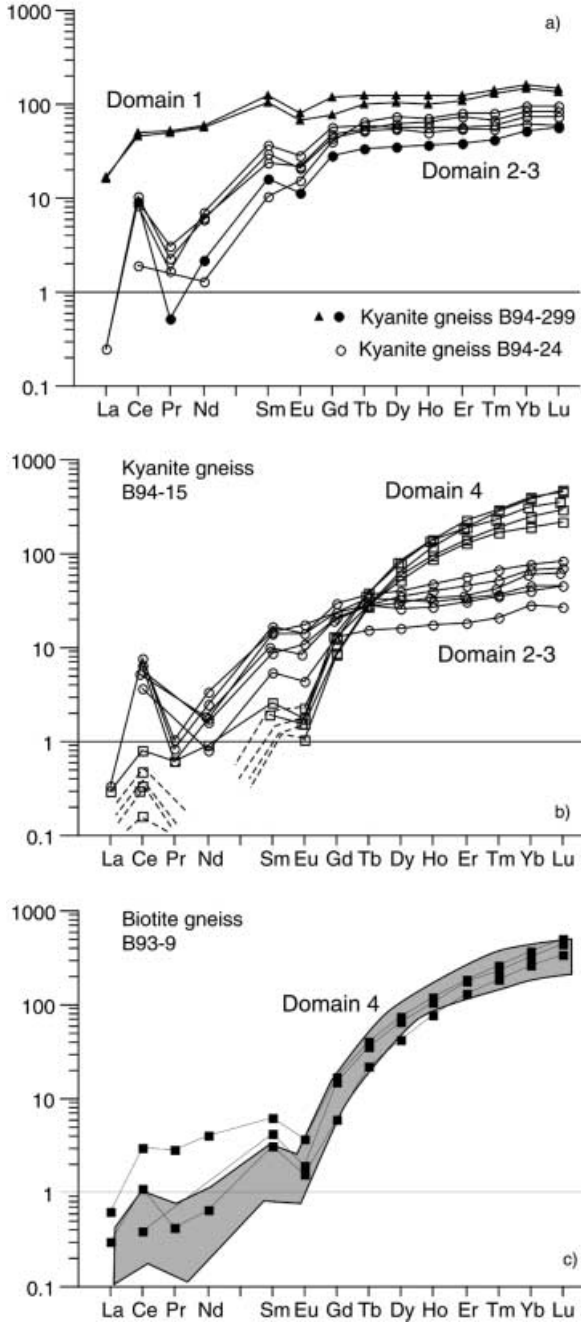

Fig. 5 REE characterisation of zircon domains. **a** Visible cores in TL (domain 1) display a different REE pattern than the metamorphic domains 2–3, indicating that the REE did not completely re-equilibrate at UHP conditions. **b** Domains 2–3 are characterised by flat REE patterns from the MREE to the HREE. This indicates that these domains formed in the presence of garnet. Domain 4 has much higher HREE contents than domains 2–3, which co-exist with garnet. **c** Idiomorphic zircon overgrowths in a biotite gneiss display very similar patterns as domain 4 in a kyanite gneiss (*shown as grey field*)

celadonite contents than phengite in the main amphibolite facies foliation (Fig. 6a). Samples B93-161 and B94-24 have no phengite in the main assemblage but do have Ti-bearing phengite as inclusions in zircon. This provides further evidence that Ti-bearing phengite formed prior to the granulite-facies equilibration. In fact, the Ti-bearing phengite displays a similar composition as HT–HP phengite produced in experiments (Patiño Douce and McCarthy 1998) and was most probably trapped in zircon during UHP conditions. Further evidence of UHP zircon formation comes from garnet and omphacite inclusions (Fig. 4e) in sample B94-299, which occurred in the same zircon domain. Garnet–clinopyroxene thermometry yields temperatures of 950 °C, which is in agreement with peak metamorphic temperatures. The garnet composition is more Mg-rich than garnet in the main assemblage (Table 3) and, in this sample, clinopyroxene only occurs as an inclusion in zircon. Additionally, the omphacite composition is completely different compared with the clinopyroxene found in the granulite-facies assemblage (Fig. 6b). These examples demonstrate that zircon is an excellent container for UHP minerals, which were completely transformed during granulite-facies equilibration in the gneisses.

Domains 2 and 3 display the same patchy to weak concentric zoning in CL (Fig. 4) and similar REE patterns. They are characterised by a nearly flat pattern from the mid-(M)REE to the HREE with a slight negative Eu-anomaly (Fig. 6). Such patterns are typical for zircon coexisting with garnet, a mineral that competes with zircon for the incorporation of HREE (Rubatto and Williams 2000). This observation is in line with the fact that garnet is present as a restite phase during decompression and isobaric cooling (Fig. 2). Rubatto and Williams (2000) argued that eclogite-facies zircon has, when compared with magmatic zircon (e.g. Hinton and Upton 1991), a very small Eu anomaly because they formed in the absence of any feldspar phase. However, the negative Eu anomaly in the Kokchetav zircons ($Eu/Eu^* = 0.6$) is more pronounced than that documented by Rubatto and Williams (2000), a difference that can be explained by distinct whole rock compositions. In fact, the Kokchetav rocks display an Eu anomaly (Shatsky et al. 1999) very similar to that of zircon domain 2 and 3.

Domain 3: upper amphibolite to granulite-facies zircon

Domain 3 is characterised by LP inclusions such as plagioclase and chlorite, which are not stable at UHP conditions (Fig. 4h). Domain 3 also contains inclusions such as K-feldspar, biotite and phengite (Fig. 6a; Table 1), which occur in the granulite to amphibolite-facies of the main paragenesis of the gneisses. These inclusions provide evidence for the formation of zircon during LP recrystallisation of the gneisses. Garnet inclusions in zircon from samples B94-24 and B94-15 are very similar to the composition of garnet in the amphibolite to granulite-facies assemblage, providing further evidence for zircon formation during this major metamorphic overprint. Most interestingly, the composition of garnet included in these zircons varies considerably (Fig. 6c, Table 3). The strong variation of mineral inclusions in zircon and the change of garnet composition within

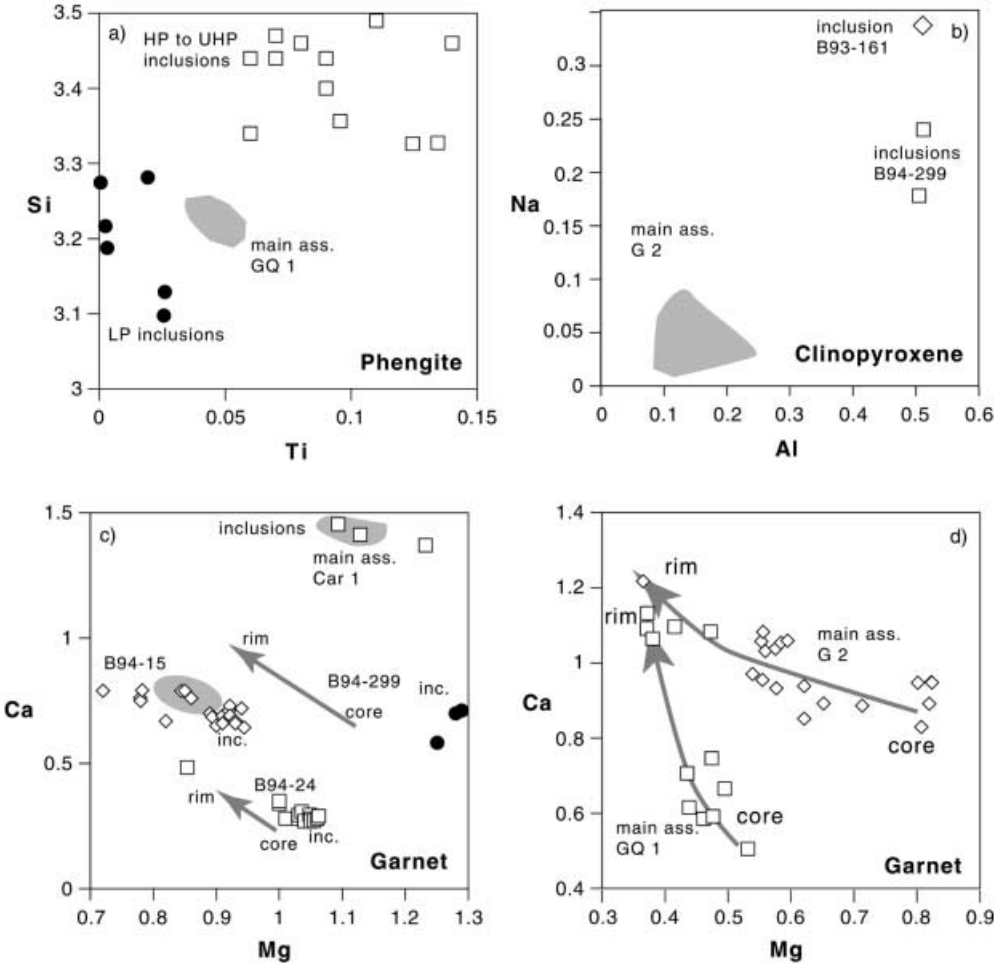

Fig. 6 Compositions of rock-forming minerals and inclusions (in cations per formula unit). **a** UHP micas are characterised by high Si and Ti contents. LP phengite, with a similar composition as the main assemblage phengite, occurs also as zircon inclusion. **b** UHP clinopyroxene inclusions in zircon have much higher Al and Na contents than clinopyroxene found in the main assemblages. **c** Comparison of garnet included in zircon (*symbols*) and in the main assemblage (*grey fields* and *arrows*). In the dolomitic metacarbonate (Car 1), inclusions display the same compositions as the UHP garnets in the main assemblage. Garnet inclusions in zircon in the kyanite–gneiss B24-299 probably formed at UHP conditions and differ from the compositional range (core to rim, *grey arrow*) in the granulite- to amphibolite-facies overprint. In the other two samples, garnet inclusions display compositions very similar to those of garnets in the main assemblage. **d** Compositional trends from core to rim in garnets are compatible with near-isobaric cooling. The different slopes of the trends are probably related to a different paragenesis. In sample GQ1, Ca may be provided by plagioclase and in G2, clinopyroxene or amphibole is probably the Ca source

zircons from one sample demonstrate that new zircon domains formed over a period of time from the UHP peak to retrograde granulite and amphibolite-facies conditions.

Domain 4: lower amphibolite-facies zircon

Some zircons display a well-developed prismatic overgrowth (domain 4) on domains 2 and 3, which is clearly distinguishable because of its dark CL emission (Fig. 4f, g). K-feldspar and biotite are occasionally included in these overgrowths. The most surprising feature is the distinct REE pattern of domain 4, which is characterised by a very steep pattern and HREE concentrations of an order of magnitude higher than domains 2 and 3 (Fig. 5). The steep pattern and the high concentration of HREE indicate that there was no other phase to fractionate the HREE and are typical for garnet-free metamorphic rocks (Rubatto et al. 2001; Rubatto and Williams 2000). Garnet was stable during the whole decompression, and continuous growth of garnet during isobaric cooling is documented by its zoning. Therefore, we suggest that crystallisation of zircon domain 4 post-dates isobaric cooling and probably occurred during lower amphibolite-facies metamorphism.

Th–U–Pb systematics

The four zircon domains were analysed by SHRIMP (ion microprobe) for Th, U and Pb. With a few exceptions, analyses of domains 1 to 3 yielded medium to low U contents (35–400 ppm; see supplementary electronic Table 1). Domain 4 generally has higher U contents up to 1,225 ppm, which is in line with lower

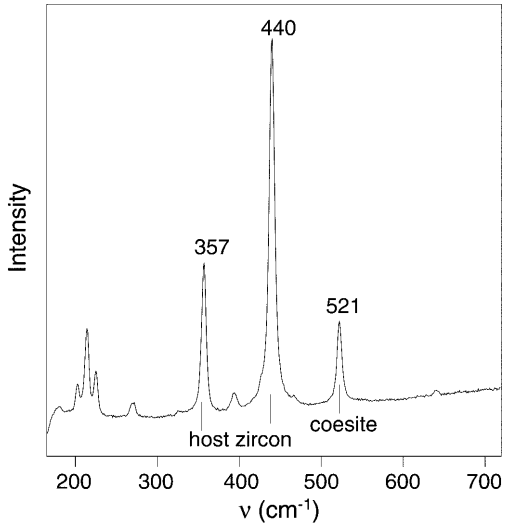

Fig. 7 Laser Raman micro-spectrometry of a coesite inclusion in zircon from the Kokchetav massif gneisses. Coesite and α-quartz are distinguishable by their Raman spectra. Coesite is characterised by a main band at 521 cm^{-1}, corresponding to the Vs(Si–O–Si) stretching mode, whereas α-quartz has its main band at 466–467 cm^{-1}

CL emission (Rubatto and Gebauer 2000). Th contents are mainly in the order of 1–10 ppm with a few analyses yielding up to 110 ppm of Th. Th/U ratios of zircon domains 2, 3, and 4 are always below 0.1, as expected for metamorphic zircon (Rubatto and Gebauer 2000). A couple of analyses of domain 1 produced higher Th/U ratios (0.15 and 0.29), comparable with the values reported by Claoue-Long et al. (1991). The higher Th/U ratios of domain 1 are consistent with their distinct REE composition in supporting the hypothesis that some zircon cores observed in TL formed prior to peak metamorphism.

The 52 SHRIMP analyses all fall in the range 514–547 Ma and are normally distributed around a mean $^{206}Pb/^{238}U$ age of 528 Ma (Fig. 8a). Although a considerable number of measurements were carried out on zircon of each domain, no age difference was detected. In particular, for domains 2, 3 and 4, the age distribution is very similar. Only the analyses for domain 1 for cumulative probability suggest a slightly older age (Fig. 8b). The analyses form a single cluster in the $^{238}U/^{206}Pb$ vs $^{207}Pb/^{206}Pb$ diagram for uncorrected data (Fig. 9). Considering only the analyses that could be classified as domains 1 to 4 on the basis of inclusions, REE pattern and CL images, the mean ages are 535 ± 9 Ma for domain 1 ($n = 6$), 527 ± 5 Ma for domain 2 ($n = 13$), 528 ± 8 Ma for domain 3 ($n = 6$) and 526 ± 5 Ma for domain 4 zircon ($n = 13$). Sixteen other zircon domains that were analysed did not contain diagnostic mineral inclusions, but, according to their CL patterns and REE composition, they formed between UHP metamorphism and granulite-facies conditions (domains 2 and 3).

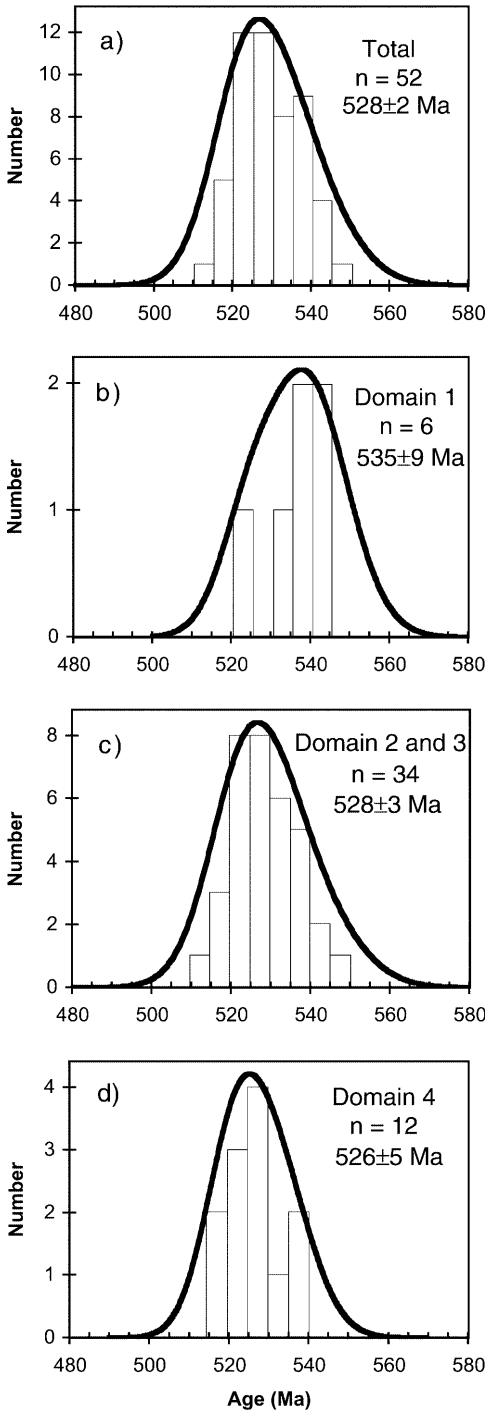

Fig. 8 Histogram with superimposed cumulative probability curves for U–Pb ages of different zircon domains and mean age of the zircon populations

Discussion

Formation or cooling ages?

The four zircon domains dated have distinct inclusions and REE compositions, which indicate formation at different stages of the Kokchetav rocks evolution. The

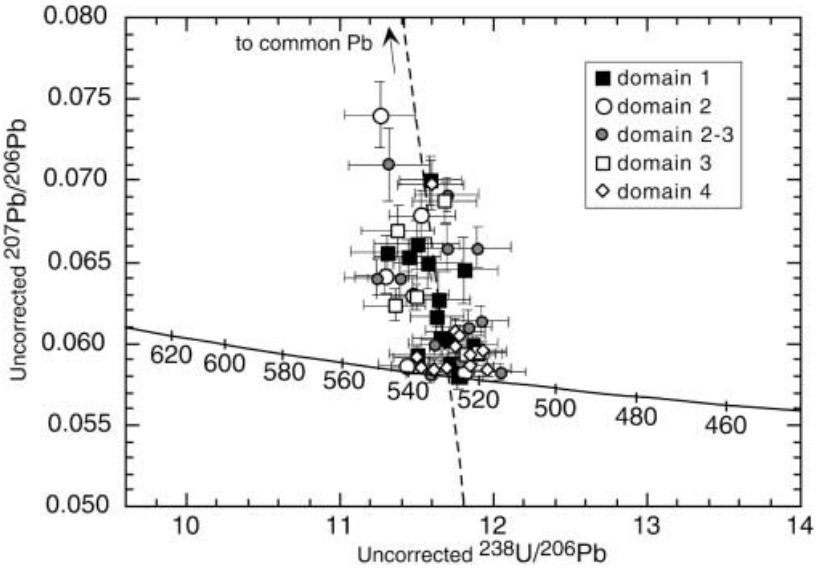

Fig. 9 Tera–Wasserburg plot for the SHRIMP analyses of the investigated zircons. *Error bars* represent 1σ errors. This presentation is preferred to a conventional concordia plot because the analyses do not define an isochron in $^{208}Pb/^{206}Pb$–Th/U space, denoting differential movement of Th and U in the metamorphic zircon (Compston et al. 1992)

undistinguishable ages of these domains could be explained by considering 528–526 Ma as a cooling age. This interpretation would also explain why visible cores in TL with no UHP inclusions (domain 1) did not record significantly older ages. However, Claoue-Long et al. (1991) reported pre-530 Ma ages from zircons of a biotite–gneiss from the Kumdy-Kol locality, demonstrating that peak metamorphic conditions of 950 °C were not sufficient to completely reset the U–Pb system of all the zircons. The tendency towards an older age (535 ± 9 Ma), the distinct REE composition and, at least in part, the high Th/U ratio of domain 1 are additional indications that older zircon cores were not completely chemically re-equilibrated during metamorphism. Preservation of original REE patterns in zircon, where the U–Pb system was partly reset, has been described by Hoskin and Black (2000). Such a feature is not surprising considering that, in zircon, at least part of the REE diffuses slower than Pb (Cherniak et al. 1997; Lee et al. 1997). However, it is also possible that the cores formed during prograde metamorphism and that their age is indistinguishable from domain 2 zircon.

Lee et al. (1997) experimentally determined that natural zircon has a closure temperature for Pb greater than 900 °C, which corresponds to a metamorphic peak in the Kokchetav rocks (domain 2) and is much higher than the temperature at which zircon domains 3 and 4 are thought to have formed. Moreover, the zircons investigated are clear and have medium to low U contents, arguing against any radiation damage that could have had favoured lead loss at relatively low temperatures. From these arguments, we conclude that zircon domains 2, 3 and 4 record formation and not cooling ages.

The age of 527 ± 5 Ma obtained from the UHP zircon domain 2 confirms the U–Pb age of 530 ± 7 Ma produced by Claoue-Long et al. (1991). Because of the fast evolution of the Kokchetav rocks, the SHRIMP data cannot clarify whether the very similar Sm–Nd age of

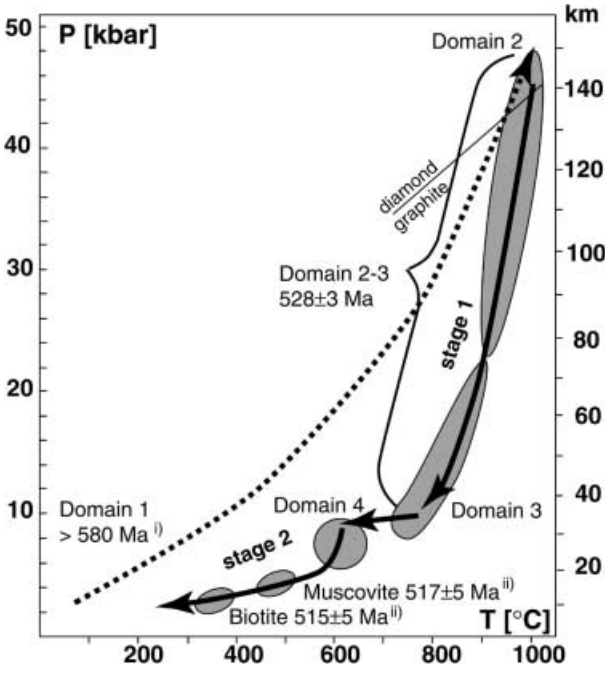

Fig. 10 P–T–t path of the Kokchetav rocks based on the correlation of different zircon domains to metamorphic conditions. (1) Inherited ages are taken from Claoue-Long et al. (1991) and (2) mica cooling ages come from Troesch and Jagoutz (1993) and Shatsky et al. (1999). Two stages of exhumation are separated from each other by a period of near-isobaric cooling

535 ± 3 Ma from mineral separates of two eclogites of unit I in the Zerenda Series (Shatsky et al. 1999) represents a formation age during prograde or a cooling age during retrograde metamorphism (see Fig. 10). A new age of the retrograde evolution of the Kokchetav rocks is defined by the zircon domain 4, which most probably formed during decompression at amphibolite-facies conditions (Fig. 10). The mean age of 526 ± 5 Ma indicates that exhumation and cooling continued after the

fast exhumation from mantle depth. This age is in good agreement with ^{39}Ar–^{40}Ar dating of muscovite and biotite from an amphibolite-facies gneiss, which gives ages of 517 ± 5 and 515 ± 5 Ma, respectively (Troesch and Jagoutz 1993; Shatsky et al. 1999).

Exhumation rate

The fact that there is no age difference between domains 2 and 3 implies that the Kokchetav rocks went from UHP conditions ($P > 43$ kbar, $T \sim 950$ °C) to amphibolite facies (9 ± 2 kbar, 650 °C) in a time interval smaller than the analytical error on the age determination. In order to estimate the maximum time span for this evolution we calculated the mean age of the zircon domains formed between the UHP peak and the granulite-facies stage (domain 2 + domain 3 + 16 analyses of domains 2–3). These analyses are normally distributed and yield a mean age of 528 ± 3 Ma (Fig. 8c). Consequently, the exhumation from > 140 km to ~ 35 km depth must have occurred within less than 6 Ma (Fig. 10). The resulting exhumation rate of 1.8 cm/year is only a minimum estimate and it is possible that the exhumation rate was considerably higher because only the minimum peak pressures and maximum time span of exhumation are known.

The calculated exhumation rate of more than 1.8 cm/year for the diamondiferous rocks demonstrates that exhumation can act at the same tectonic speed as subduction. This seems to be a common feature in exhumation of deeply subducted continental crust. Kröner et al. (2000) dated zircons from HP (> 15 kbar), MP (6–8 kbar) and LP (~ 4 kbar) granulites in the Bohemian Massif and, similar to our results, all the zircon ages were indistinguishable within error. Very high exhumation rates have been deduced for the Dora Maira Massif, Western Alps. On the basis of SHRIMP U–Pb dating of zircon with peak metamorphic inclusions ($P \sim 35$ kbar, $T \sim 750$ °C) and fission track ages of the same zircons, Gebauer et al. (1997) determined a mean exhumation rate of 2.2 cm/year. With in-situ dating of titanite crystallising at different P–T conditions, Rubatto and Hermann (2001) could demonstrate that the initial stage of exhumation was even faster and reached about 3.4 cm/year.

Implications for geochronology

The detailed study of inclusions showed that zircons with similar appearance (shape and dimension) and internal structure (CL pattern) formed over a range of metamorphic conditions. Extensive new growth of zircon, as documented by domains 2 and 3, is normally attributed to the presence of melts (Vavra et al. 1999; Rubatto et al. 2001). The available metamorphic (Fig. 2) and chemical data of the diamond-bearing rocks are in agreement with the presence of a granitic melt during decompression and probably even during part of the isobaric cooling. The granitic melt was probably saturated in Zr because there are visible zircon cores such as domain 1 and inherited zircon cores in the diamond-bearing gneisses (Claoue-Long et al. 1991). According to the experiments of Watson and Harrison (1983), Zr solubility decreases with temperature and is nearly independent of pressure. Continuous cooling therefore would have produced continuous zircon crystallisation from the melt. New zircon trapped inclusions, which document the change in P–T conditions. As zircon always grew in the presence of a granitic melt, it is not surprising that dimensions and internal structures in domains 2 and 3 are similar. Alternatively, the different zircon domains might represent a series of discrete events. It could be possible that fluids originating from dehydration reactions in the downgoing slab infiltrate the diamond-bearing rocks on their way back to the surface on top of the subduction zone (see below). As the temperature during decompression was > 800 °C (Fig. 2) a fluid influx would have triggered partial melting, which would lead to new crystallisation of zircon. Independent of whether zircons formed continuously during cooling or sporadically by fluid influx, this study demonstrates that an apparently homogeneous zircon population may not form at one single metamorphic stage but may represent a time span. Because of the fast exhumation rates of the Kokchetav rocks, SHRIMP dating could not resolve this age span. However, in slowly cooled granulite-facies terrains, the spread in zircon ages might not necessarily represent partial lead loss or analytical problems, but could document a real time span of zircon formation during cooling in the presence of melt (e.g. Williams et al. 1996, Rubatto et al. 2001).

A second process for metamorphic zircon formation during retrograde metamorphism is documented in domain 4. The steep REE pattern suggests that domain 4 crystallised at metamorphic conditions where no new garnet was formed. The Zr and HREE needed to form domain 4 might be introduced by metamorphic fluids. Alternatively, decomposition of garnet, which can contain 10's of ppm of Zr, might have liberated some of the Zr and trace elements needed to form new zircon overgrowths (e.g. Fraser et al. 1997). The REE patterns of zircon domain 4 thus provides evidence for retrograde zircon overgrowth at amphibolite-facies conditions.

Model for fast exhumation of diamondiferous rocks

The retrograde metamorphic evolution of the diamondiferous rocks together with the SHRIMP dating of the different zircon domains (Fig. 10) provide constraints for the exhumation of deeply subducted continental crust. In the following we present a two-stage exhumation model that could explain most of the features documented in this paper (Fig. 11).

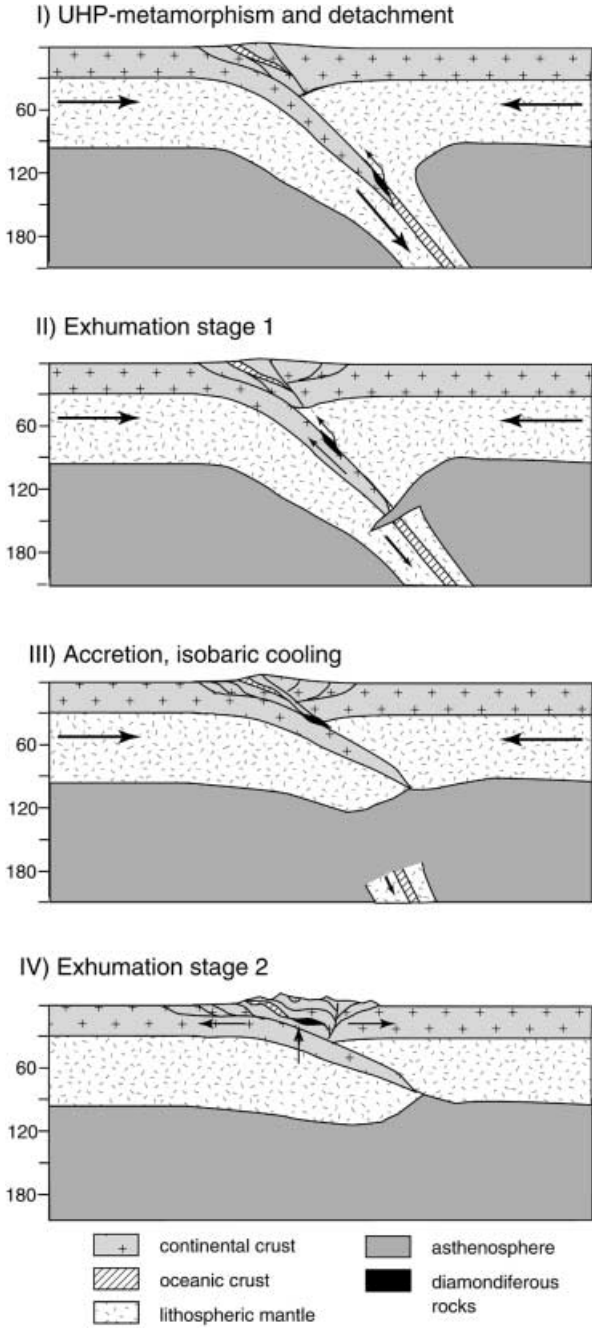

Fig. 11 Schematic sketch of a possible two-stage exhumation of the diamondiferous rocks. Subduction and first stage of exhumation are followed by continental collision and collapse of the thickened continental crust. The entire evolution took place in a time span of only about 15 Ma

UHP metamorphism and detachment

The metamorphic conditions of $P > 43$ kbar and $T \sim 950$ °C of rocks with crustal composition can only be explained by continental subduction. It is not yet solved how rocks less dense than the surrounding mantle rocks can be subducted to such a great depth. Buoyancy modelling by Cloos (1993) suggested that continental margins can be subducted to mantle depth because the bulk density of the subducted slab is dominated by dense eclogitised oceanic crust and is denser than average mantle rocks. The rock association present in the Kokchetav Massif has been thought to originate from a passive continental margin setting (Dobrzhinetskaya et al. 1994) and, therefore, this special tectonic setting might account for subduction of continental crust to diamond-facies conditions. In fact, HP to UHP metamorphism of former continent–ocean transitions has been reported from several places in the Alps (Schmid et al. 1996; Trommsdorff et al. 2000).

Exhumation stage 1

A minimum exhumation rate of 1.8 cm/year is significantly higher than fast erosion rates (Ring et al. 1999) and thus provides evidence that tectonic processes unrelated to surface uplift and erosion drove the initial exhumation. The driving force was most probably buoyancy (e.g. Platt 1993; Liou et al. 1997) of the subducted continental crust with respect to the surrounding mantle rocks. The high temperatures from diamond- to granulite-facies conditions, the mode and bulk rock composition of the diamond-bearing rocks and the widespread new growth of zircon all indicate that there was, at least sporadically, melt present during exhumation. We suggest that partial melting played a crucial role in the initiation of exhumation of these rocks. Partial melting significantly lowers the strength of the rocks and enhances the detachment of crustal slices from the downgoing slab. Additionally, partial melts might 'lubricate' contacts between the downward and upward moving rock masses and favours fast exhumation. High stress on the former continent–ocean transition because of the downward pull of the very dense eclogitic oceanic crust and the buoyant upward force of the continental crust could have resulted in slab break off (von Blankenburg and Davies 1995). The removal of dense slab material would have enhanced fast exhumation. Cooling during exhumation was greater than heat loss because of adiabatic uplift, indicating that the rocks must be exhumed on top of the slab. This is in agreement with the slab break-off model of von Blankenburg and Davies (1995), which suggests cooling during exhumation of HP rocks. The metamorphic conditions of units now outcropping adjacent to the diamondiferous rocks also display HP–LT metamorphism, but significantly lower peak pressures (unit II; Dobretsov et al. 1995; Parkinson, 2000). This indicates that slices of continental crust subducted to different depths were assembled during exhumation. This feature in the Kokchetav massif has been described as 'telescoped subduction' by Dobretsov et al. (1995) and by Zhang et al. (1997). Such nappe stacking during exhumation of UHP-continental crust has also been documented from the Dora-Maira massif in the Western Alps (Michard et al. 1993) and might be a common feature of UHP terrains.

Accretion at the base of the continental crust

Results from thermobarometry and garnets with increasing Ca contents from core to rim that co-exist with plagioclase indicate near-isobaric cooling at $\sim 9 \pm 2$ kbar after granulite-facies equilibration. We suggest that buoyancy-driven exhumation of the diamondiferous rocks stopped when they accreted at the base of the continental crust. The observation that zircon domains 3 and 4 yield the same age within the statistical error indicates fast cooling from granulite-facies (~ 800 °C) to amphibolite-facies conditions (~ 650 °C). It could be speculated that fast cooling occurred because the diamondiferous rocks were hotter than the ambient lower crustal rocks at the time of emplacement.

Exhumation stage 2

Cooling ages of muscovite and biotite are less than 10 Ma younger than equilibration of the diamondiferous rocks at lower crustal levels at the end of nearly isobaric cooling. Therefore, the rocks did not reside in the lower crust but continued their way back to the surface. This is probably related to continental collision that post-dates subduction. Collision between microcontinents has been proposed to explain the variety of rock types and metamorphic conditions in the Kokchetav massif (Dobretsov et al. 1995). Several features indicating decompression were found in amphibolite-facies gneisses containing relics of diamonds. Additionally, the diamondiferous rocks crop out in the vicinity of LP–HT rocks (unit IV, Fig. 1; Dobretsov et al. 1995). This indicates that extension related to post-collisional orogenic collapse (e.g. Vanderhaegue et al. 1999) might have played an important role in further exhumation of UHP rocks. As argued by Ring et al. (1999), uplift and erosion, which are linked to continental collision, might have been additional key factors in the final exhumation of this once deeply subducted slice of continental crust.

Conclusions

1. Mineral inclusions and trace element characteristics of zircons are powerful tools to link zircon growth to metamorphic conditions. This permits us to quantify the rates of metamorphic processes.
2. The retrograde evolution from UHP metamorphism ($P > 43$ kbar, $T \sim 950$ °C) to granulite-facies ($P \sim 10$ kbar; $T \sim 800$ °C) in the diamond-bearing rocks of the Kokchetav Massif was beyond the resolution of SHRIMP dating and occurred in a time span of less than 6 Ma.
3. Exhumation of the deeply subducted continental crust acted at a plate tectonic speed of more than 1.8 cm/year.
4. Changing mineral inclusions in zircon document the growth of zircon during several stages of the retrograde evolution. We suggest that two main processes were responsible for retrograde zircon growth: (a) cooling of Zr-saturated partial melts from UHP to granulite/upper amphibolite facies and (b) decomposition of Zr-bearing phases such as garnet at lower amphibolite-facies conditions.
5. The recognition of multistage zircon growth during retrograde metamorphic evolution indicates that the often used assumption of zircon ages representing peak metamorphic conditions must be proven by petrology and/or trace element geochemistry.
6. Zircon is an excellent container for the preservation of UHP minerals as suggested by Sobolev et al. 1994. Although the gneisses completely re-equilibrated during decompression in the presence of melts, mineral inclusions in zircons are protected from back reaction and often provide the best evidence for compositions of UHP minerals.

Acknowledgements We would like to thank F. Brink, D. Vowles and S. Stowe from the Electron Microscope Unit (ANU) and N. Ware from RSES for their help with mineral analyses and imaging, and C. Allen for assistance on the Laser-Ablation ICP-MS. This work benefited from fruitful discussions with C. De Corte and W. Taylor. Comments by two anonymous reviewers helped to improve the paper. We also thank J. Hoefs for the editorial handling. J.H. acknowledges the financial support of the Schweizerischer Nationalfonds ('Nachwuchsstipendium') and the Australian Research Council.

References

Berman RG (1988) Internally consistent thermodynamic data for minerals in the system Na_2O–K_2O–CaO–MgO–Fe_2O_3–Al_2O_3–SiO_2–TiO_2–H_2O–CO_2. J Petrol 29:445–522

Berman RG (1990) Mixing properties of Ca–Mg–Fe–Mn garnets. Am Mineral 75:328–344

Cherniak DJ, Hanchar JM, Watson EB (1997) Rare-earth diffusion in zircon. Chem Geol 134:289–301

Chopin C (1984) Coesite and pure pyrope in high grade blueschists of the western Alps: a first record and some consequences. Contrib Mineral Petrol 86:107–118

Claoue-Long JC, Sobolev NV, Shatsky VS, Sobolev AV (1991) Zircon response to diamond-pressure metamorphism in the Kokchetav Massif. Geology 19:710–713

Cloos M (1993) Lithospheric buoyancy and collisional orogens: Subduction of oceanic plateaus, continental margins, island arcs, spreading ridges, and seamounts. Geol Soc Am Bull 105:715–737

Compagnoni R, Hirajima T, Chopin C (1995) Ultra-high-pressure metamorphic rocks in the Western Alps. In: Coleman RG, Wang X (eds) Ultrahigh pressure metamorphism. Cambridge Univ Press, Cambridge, pp 206–243

Compston W, Williams IS, Kirschvink JL, Zhang Z, Ma G (1992) Zircon U–Pb ages for the Early Cambrian time-scale. J Geol Soc Lond 149:171–184

De Corte K (2000) Study of microdiamonds from UHP metamorphic rocks of the Kokchetav Massif (northern Kazakhstan): characterization and genesis. PhD Thesis, Ghent University

Dobretsov NL, Sobolev NV, Shatsky VS, Coleman RG, Ernst WG (1995) Geotectonic evolution of diamondiferous parageneses, Kokchetav Complex, northern Kazakhstan – the geologic

enigma of ultrahigh pressure rocks within a Phanerozoic fold belt. Island Arc 4:267–279
Dobrzhinetskaya LF, Braun TV, Sheshkel GG, Podkuiko YA (1994) Geology and structure of diamond bearing rocks of the Kokchetav Massif (Kazakhstan). Tectonophysics 233:293–313
Eggins SM, Rudnick RL, McDonough WF (1998) The composition of peridotites and their minerals: a laser ablation ICP-MS study. Earth Planet Sci Lett 154:53–71
Ellis DJ, Green DH (1979) An experimental study of the effect of Ca upon garnet–clinopyroxene Fe–Mg exchange equilibria. Contrib Mineral Petrol 71:13–22
Fraser G, Ellis D, Eggins S (1997) Zirconium abundance in granulite-facies minerals, with implications for zircon geochronology in high-grade rocks. Geology 25:607–610
Fuhrman ML, Lindsley DH (1988) Ternary-feldspar modelling and thermobarometry. Am Mineral 73:201–216
Gebauer D, Schertl HP, Brix M, Schreyer W (1997) 35 Ma old ultrahigh-pressure metamorphism and evidence for very rapid exhumation in the Dora Maira Massif, Western Alps. Lithos 41:5–24
Ghent ED (1976) Plagioclase–garnet–Al_2SiO_5–quartz: a potential geobarometer-geothermometer. Am Mineral 61:710–714
Graham CM, Powell R (1984) A garnet–hornblende geothermometer: calibration, testing and application to the Pelona schist, southern California. J Metamorph Geol 2:13–31
Green TH, Hellman PL (1982) Fe–Mg partitioning between coexisting garnet and phengite at high pressures, and comments on garnet–phengite geothermometer. Lithos 15:253–266
Hermann J, Green DH (1999): Experimental constraints on continental rocks in ultra-high pressure metamorphism. LPI Contribution no 971, pp 123–124
Hermann J, Green DH (2000): Experimental constraints on fluid absent melting in deeply subducted crust. J Conf Abstr 5(1):48
Hermann J, Müntener O, Trommsdorff V, Hansmann W, Piccardo GB (1997): Fossil crust to mantle transition, Val Malenco (Italian Alps). J Geophys Res 102(B9):20123–20132
Hinton RW, Upton BGJ (1991) The chemistry of zircon: variations within and between large crystals from syenite and alkali basalt xenoliths. Geochim Cosmochim Acta 55:3287–3302
Holdaway MJ (1971) Stability of andalusite and the aluminium silicate phase diagram. Am J Sci 271:97–131
Hoskin PWO, Black LP (2000) Metamorphic zircon formation by solid-state recrystallization of protolith igneous zircon. J Metamorph Geol 18:423–439
Hunziker JC, Desmond J, Hurford AJ (1992) Thirty-two years of geochronological work in the Central and Western Alps: a review on seven maps. Mém Géol (Lausanne) 13:1–59
Indares A, Martignole J (1985): Biotite–garnet geothermometry in the granulite facies: the influence of Ti and Al in biotite. Am Mineral 70:272–278
Kennedy CS, Kennedy GC (1976) The equilibrium boundary between graphite and diamond. J Geophys Res 81:2467–2470
Korsakov A (2000) The petrology of metamorphic diamondiferous rocks from Barchi-Kol area Kokchetav Massif (northern Kazahstan). PhD Thesis, Institute Mineralogy and Petrography SB RAS, Novosibirsk
Kröner A, O'Brien PJO, Nemchin AA, Pidgeon RT (2000) Zircon ages for high pressure granulites from South Bohemia, Czech Republic, and their connection to Carboniferous high temperature processes. Contrib Mineral Petrol 138:127–142
Lee JKW, Williams IS, Ellis DJ (1997) Pb, U and Th diffusion in natural zircon. Nature 390:159–161
Liou JG, Maruyama S, Ernst WG (1997) Seeing a mountain in a grain of garnet. Science 276:48–49
Massonne H, Schreyer W (1987) Phengite geobarometry based on the limiting assemblage with K-feldspar, phlogopite, and quartz. Contrib Mineral Petrol 96: 212–224
Michard A, Chopin C, Henry C (1993) Compression versus extension in the exhumation of the Dora-Maira coesite-bearing unit, Western Alps. Tectonophysics 221:173–193
Mirwald PW, Massone HJ (1980) The low-high quartz and quartz-coesite transition to 40 kbar between 600 °C and 1,600 °C and some reconnaissance data on the effect of $NaAlO_2$ component on the low quartz-coesite transition. J Geophys Res 85:6983–6990
Parkinson CD (2000) Coesite inclusions and prograde compositional zonation of garnet in whiteschist of the HP-UHPM Kokchetav Massif Kazakhstan: a record of progressive UHP metamorphism. Lithos 52:215–233
Patiño Douce AE, McCarthy TC (1998) Melting of crustal rocks during continental collision and subduction. In: Hacker BR, Liou JG (eds) When continents collide: geodynamics and geochemistry of ultrahigh-pressure rocks. Kluwer, Dordrecht, pp 27–55
Platt JP (1993) Exhumation of high pressure rocks: a review of concepts and processes. Terra Nova 5:119–133
Ring U, Brandon MT, Willett SD, Lister GS (1999) Exhumation processes. In: Ring U, Brandon MT, Lister GS, Willett SD (eds) Exhumation processes: normal faulting, ductile flow and erosion. Geological Society Special Publication, London, pp 1–27
Rubatto D, Gebauer D (2000) Use of cathodoluminescence for U–Pb zircon dating by ion microprobe: some examples from the Western Alps. In: Pagel M, Barbin V, Blanc P, Ohnenstetter D (eds) Cathodoluminescence in geosciences. Springer, Berlin Heidelberg New York, pp 373–400
Rubatto D, Hermann J (2001) Exhumation as fast as subduction? Geology 29:3–6
Rubatto D, Williams IS (2000) Imaging, trace element geochemistry and mineral inclusions: linking U–Pb ages with metamorphic conditions. EOS Trans 21:25
Rubatto D, Williams IS, Buick IS (2001) Zircon and monazite response to prograde metamorphism in the Reynolds Range, central Australia. Contrib Mineral Petrol 140:458–468
Schmid SM, Pfiffner OA, Froitzheim N, Schönborn G, Kissling E (1996) Geophysical–geological transect and tectonic evolution of the Swiss–Italian Alps. Tectonics 15:1036–1064
Schmidt MW, Vielzeuf D (2000) Differential melt productivity of MORB, greywacke and pelite during subduction. J Conf Abstr 5(1):92–93
Shatsky VS, Sobolev NV, Vavilov MA (1995) Diamond-bearing metamorphic rocks of the Kokchetav Massif (northern Kazakhstan). In: Coleman RG, Wang X (eds) Ultrahigh pressure metamorphism. Cambridge Univ Press, Cambridge, pp 427–455
Shatsky VS, Theunissen K, Dobretsov NL, Sobolev NV (1998a) New indicator of ultrahigh-pressure metamorphism in the mica schists of the Kulet site of the Kokchetav Massif (North Kazakhstan) (in Russian). Russian Geol Geophys 39:942–955
Shatsky VS, Rylov GM, Efimova ES, de Corte K, Sobolev NV (1998b) Morphology and real structure of microdiamonds from metamorphic rocks Kokchetav Massif, kimberlites, and alluvial placers (in Russian). Russian Geol Geophys 39:1039–1044
Shatsky VS, Jagoutz E, Sobolev NV, Kozmenko OA, Parkhomenko VS, Troesch M (1999) Geochemistry and age of ultrahigh pressure metamorphic rocks from the Kokchetav Massif (northern Kazakhstan). Contrib Mineral Petrol 137:185–205
Sobolev NV, Shatsky VS (1990): Diamond inclusions in garnets from metamorphic rocks: a new environment for diamond formations. Nature 343:742–746
Sobolev NV, Shatsky VS, Vavilov MA, Goryanov SV (1994) Zircon from ultrahigh-pressure metamorphic rocks of folded regions as an unique container of inclusions of diamond, coesite and coexisting minerals (in Russian). Dokl Akad Nauk 334:482–488
Taylor WR, Canil D, Milledge HJ (1996) Kinetics of Ib to IaA nitrogen aggregation in diamond. Geochim Cosmochim Acta 60:4725–4733
Troesch M, Jagoutz E (1993) Mica cooling ages of diamond-bearing gneiss from the Kokchetav Massif, Kazakhstan. Terra Abstr EUG 7:396
Trommsdorff V, Hermann J, Müntener O, Pfiffner M, Risold AC (2000) Geodynamic cycles of subcontinental lithosphere in the Central Alps and the Arami enigma. J Geodyn 30:77–92
Vanderhaegue O, Burg JP, Teyssier C (1999) Exhumation of migmatites in two collapsed orogens: Canadian Cordillera and

French Variscides. In: Ring U, Brandon MT, Lister GS, Willett SD (eds) Exhumation processes: normal faulting, ductile flow and erosion. Geological Society Special Publication, London, pp 181–204

Vavra G, Gebauer D, Schmid R, Compston W (1996) Multiple growth and recrystallization during polyphase Late Carboniferous to Triassic metamorphism in granulites of the Ivrea Zone (Southern Alps): an ion microprobe (SHRIMP) study. Contrib Mineral Petrol 122:337–358

Vavra G, Schmid R, Gebauer D (1999) Internal morphology, habit and U–Th–Pb microanalysis of amphibolite-to-granulite facies zircons: geochronology of the Ivrea Zone (Southern Alps). Contrib Mineral Petrol 134:380–404

Vielzeuf D, Holloway JR (1988) Experimental determination of the fluid-absent melting relations in the pelitic system. Contrib Mineral Petrol 98:257–276

von Blankenburg F, Davies JH (1995) Slab break-off: a model for syncollisional magmatism and tectonics in the Alps. Tectonics14:120–131

Watson BE, Harrison MT (1983) Zircon saturation revisited: temperature and composition effects in a variety of crustal magma types. Earth Planet Sci Lett 64:295–304

Williams IS, Buick IS, Cartwright I (1996) An extended episode of early Mesoproterozoic metamorphic fluid flow in the Reynolds Range, central Australia. J Metamorph Geol 14:29–47

Zhang RY, Liou JG, Ernst WG, Coleman RG, Sobolev NV, Shatsky VS (1997) Metamorphic evolution of diamond-bearing and associated rocks from the Kokchetav Massif, Northern Kazakhstan. J Metamorph Geol 15:479–496